Interface shear capacity of veneer-based cross-laminated timber glued-in rod splice connections

Steven Kontra
Structural Designer, KL&A Engineers and Builders
Email: skontra@klaa.com

Andre R. Barbosa *
Cecil and Sally Drinkward Professor in Structural Engineering, School of Civil and Construction Engineering,
Oregon State University. Email: andre.barbosa@oregonstate.edu

Reid B. Zimmerman
Technical Director, KPFF Consulting Engineers
Email: reid.zimmerman@kpff.com

Steve Pryor
Advanced Research and Development, Simpson Strong-Tie
Email: spryor@strongtie.com

Christopher Higgins
Professor, School of Civil and Construction Engineering, Oregon State University
Email: chris.higgins@oregonstate.edu

Arijit Sinha †
JELD-WEN Chair and Professor, Dept of Wood Science and Engineering
Oregon State University. Email: arijit.sinha@oregonstate.edu

(Received 3 March 2026)

Abstract: North America's engineered mass timber sector has expanded rapidly in the past decade, with growing adoption of mass timber products as structural components in tall buildings. Among these, mass timber panels have emerged as viable shear wall elements for lateral force-resisting systems. In taller balloon-type or self-centering rocking wall constructions, panels are stacked vertically, necessitating reliable splice connections between adjacent panels. This paper introduces a novel glued-in rod (GiR) splice connection for vertical joints between stacked panels, featuring a two-stage adhesive installation process and a filler/weep hole system designed to promote full adhesive penetration and accommodate construction tolerances. An experimental program was conducted to evaluate the interface shear strength of GiRs embedded in veneer-based cross-laminated timber under both monotonic and reversed-cyclic loading. Unlike previous studies that focused on tensile strength or monotonic loading only, this work investigates shear behavior relevant to seismic and wind demands. Experimental results are compared against conservative yield strength predictions from the U.S. National Design Specification for Wood Construction (NDS) dowel-type equations. Findings offer new insights into the shear performance of GiR splices in veneer-based cross-laminated timber, informing design assumptions for vertical panel joints in balloon-type mass timber wall systems and providing experimentally validated allowable loads for seismic design.

Keywords: Glued-in rods; Interface shear; Mass ply panel; Shear wall; Splice connection; Veneer-based cross-laminated timber

Introduction

The continued advancement of mass timber engineered wood products provides architects and engineers with a wide range of design solutions. Among these, the use of mass timber panel elements in floor diaphragms and shear walls has emerged as a promising strategy for achieving both sustainability and structural resilience (Tannert et al. 2018; Izzi et al. 2018; Sun et al. 2020; Granello et al. 2020; Di Cesare et al. 2020; Abed et al. 2022). These developments have enabled mass timber to be considered as a primary structural material for mid- and high-rise buildings. However, challenges remain, particularly in implementing mass timber panels in tall structures (Pei et al. 2016). A key limitation stems from manufacturing and transportation constraints, which restrict panel lengths. In tall balloon-frame wall systems, for instance, the required wall height may exceed the available panel length, necessitating vertical stacking and the use of splice connections at panel joints

* Corresponding author
† Society of Wood Science & Technology member

https://doi.org/10.22382/wfs-2026-17

to ensure structural continuity. Therefore, the performance and reliability of panel splice connections have become a critical focus of research and design. Figure 1 illustrates this need, showing a rendering of a 10-story mass timber shake-table test building (Pei et al. 2024), where splice connections are required to form continuous balloon-type shear walls.

Several design alternatives have been proposed for splice connections in balloon-type mass timber shear walls. Two conceptual examples are illustrated in Figure 2. In the first configuration (Figure 2a), six steel plates are fastened externally across the panel joint. In this design, the end plates are typically assumed to resist overturning moments, while the central plates carry shear forces (Zimmerman et al. 2020). The second configuration (Figure 2b) utilizes glued-in rods (GiRs) to transfer forces across the splice in a similar manner. In design, the GiRs are grouped according to their function: longer rods embedded near the panel ends can be assumed to resist overturning moments, while shorter, centrally located rods are assumed to resist shear.

Both splice types shown in Figure 2 are viable. The steel plate connection offers the advantage of rapid on-site assembly but

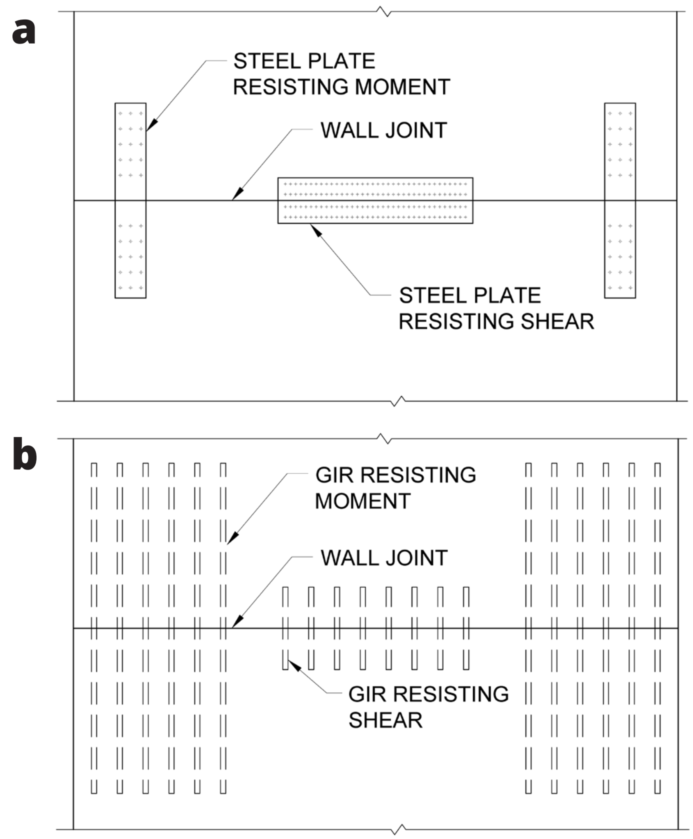

Figure 2. Examples of mass timber wall splice connections: (a) external steel plates; (b) internal GiRs.

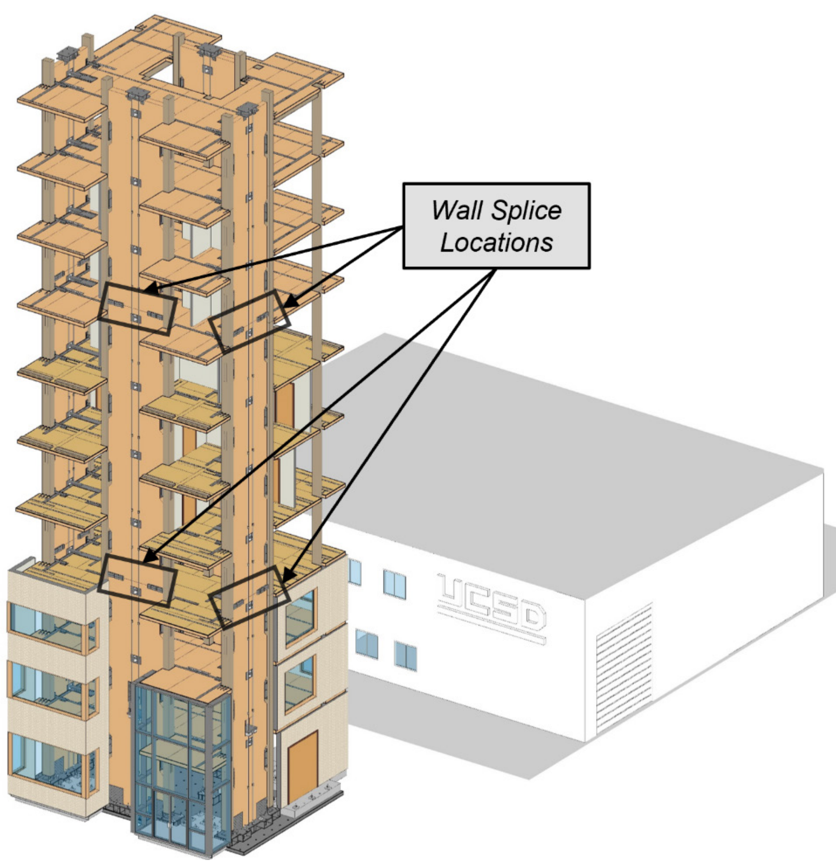

Figure 1. Mass timber wall splice locations along the building height (adapted from Pei et al. 2024).

requires additional measures for corrosion and fire protection. In contrast, the GiR connection provides benefits such as improved corrosion and fire resistance, enhanced aesthetics, and favorable ductile behavior under seismic loading (Townsend et al. 1990), making it an attractive option for designers. However, GiR connections demand greater prefabrication effort, as precise hole alignment is necessary for proper rod placement—especially challenging for longer embedded lengths. Moreover, successful installation requires controlled environmental conditions and skilled application to ensure proper adhesive bonding between the rods and the mass timber substrate. Based on the design premise presented in the previous paragraph, when designing the GiR splice connection to resist lateral loads from both wind and seismic actions, the main design considerations are that the moment-resisting outer rods produce an internal force couple, which places individual rods in tension (and potentially some compression), while the central rods resist shear forces and provide lateral stiffness.

Glued-in rod connections were originally developed for glue-laminated timber, where their axial (pull-out) capacity and, to a lesser extent, their lateral (shear) and combined load-carrying behavior have been experimentally characterized (Deng 1997; Bengtsson and Johansson 2002; Jensen and Gustafsson 2004; Steiger et al. 2007; Jensen and Quenneville 2009). More recently, the axial and bond performance of GiRs has been investigated in cross-laminated timber (Azinović et al. 2018; Sofi et al. 2021; Ayansola et al. 2022), and the tension pull-out capacity of single GiRs has been quantified in mass ply panel (MPP) (Field et al. 2023). GiR splice connections are attractive for vertical panel-to-panel joints because the rods are fully embedded within the panels, providing improved corrosion and fire resistance, enhanced aesthetics, and ductile behavior relative to externally fastened steel-plate splices (Townsend et al. 1990; Zimmerman et al. 2020). In contrast, the behavior of GiR connections loaded in interface shear, especially under reversed-cyclic demands and in the panel-to-panel splice configuration studied here, has received comparatively little attention. The present study addresses this gap by characterizing the interface shear capacity, stiffness, and cyclic response of GiR splice connections in MPP and by comparing the observed response with U.S. National Design Specification for Wood Construction (NDS) yield predictions (AWC 2018).

Previous research has studied the behavior of GiRs in tension in a variety of timber substrates. Bengtsson and Johansson (2002), Deng (1997), and Steiger et al. (2007) investigated the structural performance in a glue-laminated timber substrate; Ayansola et al. (2022), Azinović et al. (2018), and Sofi et al. (2021) in a cross-laminated timber (CLT) substrate; and Field et al. (2023) in an MPP (ICC-ES 2022) substrate. The experimental program presented in Field et al. (2023) characterized the pull-out tensile strength and stiffness of a single GiR at different levels of embedment. Test results were used to propose a design equation with a format that is similar to the ones available in the New Zealand design code (NZS 3603 1993), which is based on work developed in Deng (1997), among others.

With respect to the behavior of GiRs in shear in timber substrates, several experimental and analytical modeling efforts are available in the literature. Bengtsson and Johansson (2002) evaluated steel-threaded GiRs embedded into glulam specimens as part of the Glued-in Rods for Timber Structures (GIROD) project used to promote code adoption of this connection type in Europe. The objective of the study was to investigate the effect of rod spacing and edge distance on the axial and lateral load-carrying capacity. For the lateral loading tests, rods were glued-in at a length of 320 mm parallel to the grain of glulam specimens with varied edge distances. For some specimens, low-strength rods were installed to investigate the influence of steel quality on lateral load-carrying capacity. For low-strength rods particularly, two plastic hinges were observed to form in the rods during testing. When the edge distance was decreased, larger embedding displacements in the timber were observed. Jensen and Gustafsson (2004) and Jensen and Quenneville (2009) validated this conclusion through experimental analysis and modeling of a GiR shear connection of dowels embedded in glulam. In both works, different joint parameters were evaluated with varying glulam geometries, as well as dowel quantities and placement, ultimately confirming that increasing edge distance increased observed shear strength. From these test programs, the minimum edge distance was 2 rod diameters (d), from which an initial testing plan could conceivably be developed based on this minimum distance to provide a lower bound for expected capacity of GiRs in shear.

This research for both tension and shear loading has helped to establish parameters for detailing GiR connections. In state-of-the-art reviews, Steiger et al. (2015) and Tlustochowicz et al. (2011) summarized several important recommendations as follows: target edge distance of 2.5d with a lower bound of 2d, rod spacing minimum of 5d, and an upper bound glue-line thickness of 2 mm. Three adhesives were also listed that have been utilized most prominently for GiR connections: polyurethane (PUR), phenol resorcinol (PRF), and epoxy resins (EPX), where it was noted that EPX developed an especially strong bond with the steel and wood. A study by Xu et al. (2020) pointed out that some uncertainty can arise in the strength of these connections due to panel manufacturing defects that lead to panel voids, underscoring the necessity for the careful selection and application of adhesive in order to maximize the strength of the bonded connection.

In shear design, the European Yield Model (EYM) developed by Johansen (1949) serves as the basis for calculating the lateral load-resisting capacity of the embedded dowels in timber. This EYM established several parameters that are needed for characterizing the embedment strength, including bearing resistance, dowel size, and loading angle. The model has been used extensively to predict the shear strength of embedded dowels in a variety of timber substrates, including glue-laminated timber (Stamatopoulos et al. 2022), CLT (Uibel and Blaß 2006), and laminated-veneer lumber (Bader et al. 2016).

Mass ply panel is a veneer-based cross-laminated timber panel fabricated from nominal 25.4 mm (1 in.) Douglas-fir veneers assembled in cross-laminated layups in accordance with ANSI/APA PRG 320 (APA 2025) and ESR-4760 (ICC-ES 2022). This veneer-based assembly produces a homogeneous layup with lower variability than sawn-lumber-based CLT. Relative to lumber-based CLT wall panels, MPP provides greater dimensional stability and higher in-plane shear stiffness for an equivalent panel thickness, owing to the absence of the gaps and lumber-layer discontinuities present in lumber-based CLT and the elimination of strength-reducing characteristics such as knots and slope of grain that can govern shear capacity. Relative to structural insulated panels (SIP) and plywood-sheathed light-frame walls, for example, MPP offers a solid, mass timber panel capable of carrying significant in-plane shear without reliance on fasteners between a frame and sheathing. These attributes make MPP well suited to wall applications requiring high in-plane stiffness and strength and serve as motivation for the development of high-capacity, internally embedded splice connections such as the GiR connections studied here. Recently, experiments have been performed to determine the embedment strength in MPP using the half-hole method prescribed in ASTM D5764 (ASTM International 2018). Miyamoto et al. (2020) evaluated the embedment strength of MPP with screws, nails, and bolts in different orientations. While bolts were not tested along the ply (loading parallel to the plane of the veneer, and perpendicular to the strong axis), screws and nails were tested in this orientation, and an average strength of 18 MPa was recorded.

Generalized yield limit equations were developed based on the EYM (AWC 2014, 2018) to predict yield strengths for dowel-based connections in single and double shear. Table 1 shows a schematic of the six different yield modes and the corresponding equations for single shear, whereby the predicted yield strength for each dowel was determined by taking the lowest result from the six yield mode equations. Note that to determine the reference lateral design values, the predicted yield strength equations shown in Table 1 were divided by a reduction term, R_d, that is listed in the NDS Table 12.3.1B (AWC 2018). This term converts the theoretical yield load predicted by each EYM equation into a reference lateral design value consistent with the NDS allowable stress design (ASD). R_d is mode-specific and accounts for the ratio between the load at first yield and the load corresponding to the reference deformation limit of 0.381 mm (0.015 in.), as well as the format conversion from the Load and Resistance Factor Design (LRFD) basis of the yield model. Applying R_d ensures the resulting reference design value reflects appropriate deformation and safety levels for dowel-type connections. For Mode III_s, III_m, and IV, and for dowels with diameter between 6.35 mm (0.25 in.) and 25.4 mm (1 in.), the R_d is given by:

$$R_d = 3.2\ K_\theta \qquad [1]$$

where $K_\theta = 1 + 0.25(\theta/90)$, and θ is equal to the maximum angle between the direction of load and the direction of grain for any member in the connection ($0° \leq \theta \leq 90°$).

Prior work has extensively characterized tension capacity of GiRs in timber substrates and, to a lesser extent, monotonic shear behavior. However, reversed-cyclic shear response of GiR splices in MPP for vertical joints remains unexplored. Thus, the main objectives of this work are to:

1. quantify interface shear capacity and stiffness under monotonic and cyclic loading;
2. assess the influence of joint interface adhesion (unintended adhesive at the panel interface) on strength and stiffness; and
3. compare observed yield to NDS predictions (AWC 2018) and report design values following ICC-AC526 (ICC-ES 2021).

Materials and methods

Specimen design

Eleven MPP specimens were fabricated for the experimental program. The panels used in this study were grade F16, fabri-

Table 1. Yield modes and predicted yield strength per NDS (AWC 2018).

Yield Mode	Equation	Eq. No.
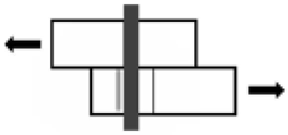 (I_m)	$P = D\, l_m\, F_{em}$	[2]
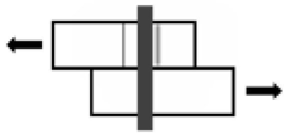 (I_s)	$P = D\, l_s\, F_{es}$	[3]
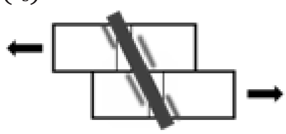 (II)	$P = k_1\, D\, l_s\, F_{es}$ where: $k_1 = \frac{\sqrt{R_e + 2\,R_e^2\,(1+R_t+R_t^2) + R_t^2\,R_e^3} - R_e\,(1+R_t)}{(1+R_e)}$	[4]
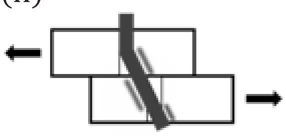 (III_m)	$P = k_2\, D\, l_m\, F_{em}$ where: $k_2 = -1 + \sqrt{2\,(1+R_e) + \frac{2\,F_{yb}\,(1+2\,R_e)\,D^2}{3\,F_{em}\,l_m^2}}$	[5]
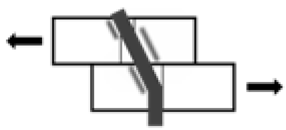 (III_s)	$P = \frac{k_3\, D\, l_s\, F_{em}}{(2+R_e)}$ where: $k_3 = -1 + \sqrt{\frac{2\,(1+R_e)}{R_e} + \frac{2\,F_{yb}\,(2+R_e)\,D^2}{3\,F_{em}\,l_s^2}}$	[6]
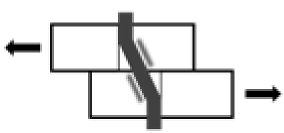 (IV)	$P = D^2 \sqrt{\frac{2\,F_{em}\,F_{yb}}{3\,(1+R_e)}}$	[7]
where:	P = predicted yield strength	
	D = dowel diameter (in.)	
	F_{yb} = dowel bending yield strength (psi)	
	$R_e = F_{em} / F_{es}$	
	$R_t = l_m / l_s$	
	l_m = main member dowel bearing length (in.)	
	l_s = side member dowel bearing length (in.)	
	F_{em} = main member dowel bearing strength (psi)	
	F_{es} = side member dowel bearing strength (psi)	

cated from 1.6E Douglas-fir veneers with an equivalent specific gravity of approximately 0.42 (ESR-4760). As shown in Figure 3, each specimen consisted of two 102-mm-thick grade F16-4 MPP parts, including a custom-cut top section (Part A) and a rectangular bottom section (Part B). The shape of the specimens allowed for the line of action of the actuator-applied load to act collinearly with the interface between the two parts (i.e., no imposed moment at the panel-to-panel interface). Parts A and B were connected using three 25.4 mm (1 in.) diameter × 406 mm (16 in.) long ASTM F1554 Grade 36 (248 MPa [36 ksi]) rods centered in the panel thickness and embedded 203 mm (8 in.) into each part. The rods were partially threaded on

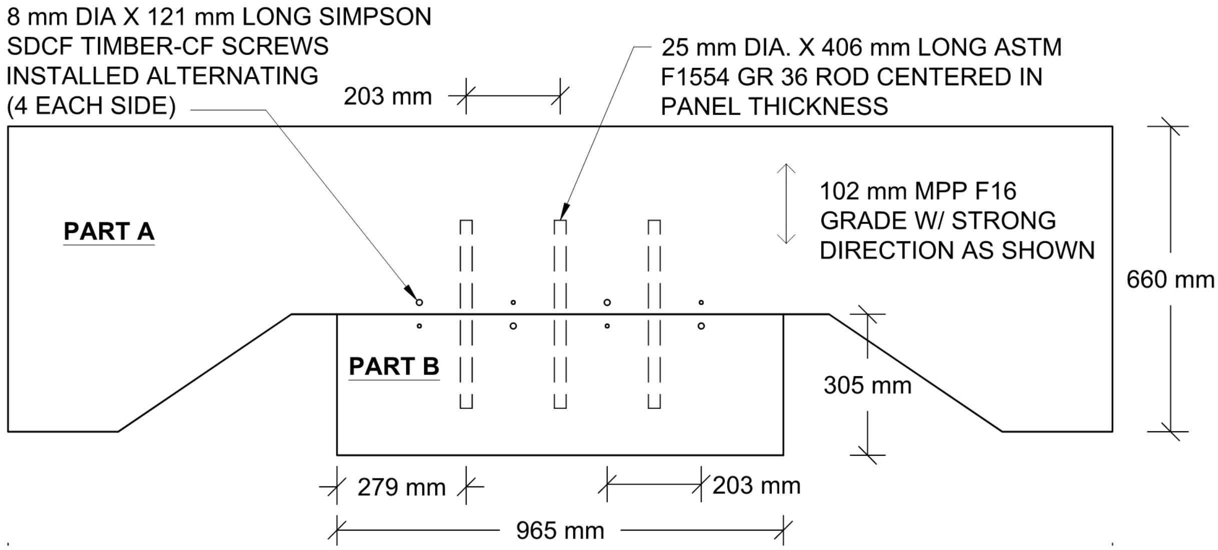

Figure 3. Specimen geometry.

the ends over a length of 102 mm (4 in.), leaving a 203 mm (8 in.) unthreaded (smooth) length in the middle of the rod. The outer rods were nominally spaced 279 mm (11 in.) from the edge of Part B and nominally spaced between rods 203 mm (8 in.) on-center.

The position of the rods created an edge distance of 2d (51 mm; 2 in.), the minimum edge distance tested in the literature (Steiger et al. 2015). This allowed characterization of a lower-bound capacity. Rods were installed in 32 mm (1-1/4 in.) diameter by 216 mm (8-1/2 in.) long holes in each panel and bonded to the MPP with structural epoxy in the vertical position. The holes were oversized by 6.35 mm (0.25 in.) relative to the diameter of the rods, resulting in a glue-line thickness of 3.175 mm, exceeding the largest recommended glue-line thickness of 2 mm in the prior literature (Steiger et al. 2015). This larger glue-line thickness represented an upper-bound condition expected in practice, which may be needed, such as in the case of construction tolerances of mass timber wall splice connections to accommodate the simultaneous installation of dozens of long threaded rods into both panels. Four 8 mm (5/16 in.) diameter by 121 mm (4-3/4 in.) long Simpson SDCF Timber-CF (fully threaded) screws were installed in an alternating pattern on each side of the specimen to restrain out-of-plane panel cracking and dilation.

Each rod was embedded 203 mm (8 in.) into each panel, corresponding to an embedment-to-diameter ratio of approximately 8 for the 25.4 mm (1 in.) diameter rods. This embedment was selected so that the rods would be sufficiently anchored to develop their full lateral (dowel) capacity and form plastic hinges under interface shear, rather than failing by rod pull-out or loss of adhesive anchorage. The selected length was consistent with guidance that the bonded length be sufficient to mobilize the stiffness and strength of the surrounding timber (Steiger et al. 2015) and with embedment-to-capacity relationships established for axially loaded GiRs in MPP (Field et al. 2023). It was also compatible with the available panel thickness and with the rod sizes adopted for the GiR splice connections in the companion six-story shake-table study (Kontra et al. 2026).

Specimen fabrication

The grade F16-4 MPP were manufactured by Freres Engineered Wood, Inc. (Lyons, OR USA). Parts were milled and machined to size at A.A. “Red” Emmerson Laboratory at Oregon State University (OSU, Corvallis, OR), then shipped to Timberlab in Portland, OR for GiR installation and specimen assembly. Specimens were then delivered back to OSU for testing in the Structural Engineering Research Laboratory at the O.H. Hinsdale Wave Research Laboratory.

The GiR installation procedure was the same for all shear specimens. Figure 4 illustrates a multi-step process that was developed for administering adhesive into the GiR connection to facilitate uniform and complete bonding of the rod and MPP. First, before applying any adhesive, holes were drilled and then cleaned using a round wire brush and compressed air to remove any free particles in both Part A and Part B. Second, a small amount of high viscosity adhesive was applied to the surface of the holes to fill any voids in the MPP so that the injected low-viscosity epoxy was confined to the area around the rod and did not disperse into the interior voids in the panel.

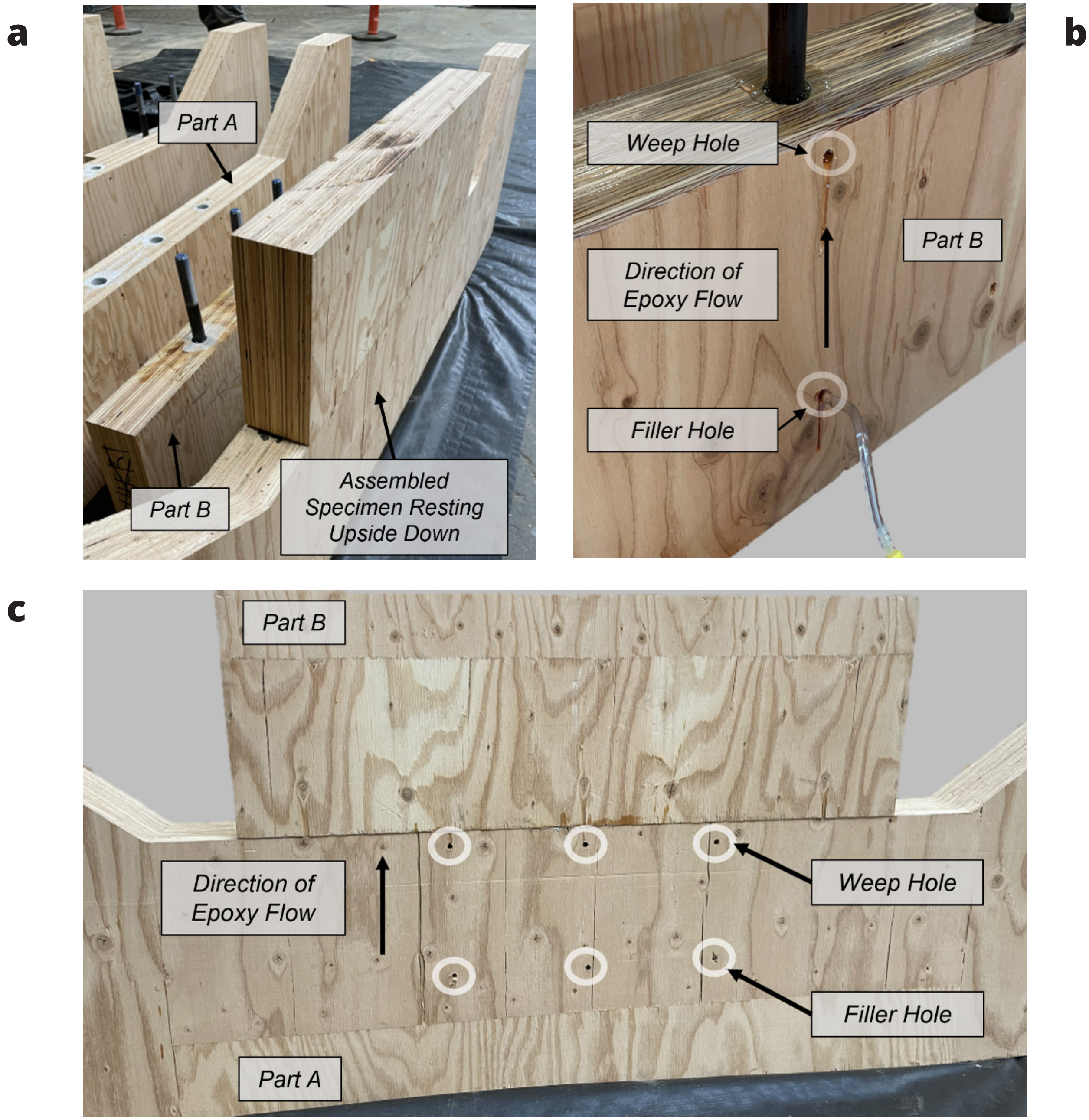

Figure 4. Specimen fabrication process: (a) Part A with first coat applied to the holes, Part B with rods installed, assembled specimen resting upside down relative to specimen geometry in Figure 3; (b) filler and weep hole in Part B; (c) filler and weep hole and direction of flow for Part A.

A custom-designed drill "spreader" attachment was used to evenly spread the adhesive to the wall of the rod holes. This was accomplished by plunging the spreader attachment on the end of a long drill rod into a small amount of adhesive at the bottom of the hole and then slowly extracting, while simultaneously spinning the spreader. The first coat of adhesive, indicated in Figure 4a, was left to cure for approximately 24 h. The adhesive used to coat the holes in this first step was designated as CI-GV epoxy gel (Simpson Strong-Tie 2023a).

After the adhesive had cured, 9.5 mm (3/8 in.) diameter holes were drilled 25.4 mm (1 in.) from each end of the rod holes to serve as the "filler" and "weep" holes, where the adhesive was injected in the filler hole and flowed out the weep hole. Any debris from drilling the filler and weep holes was cleaned out with compressed air. The threaded rods were then placed into the holes in Part B, and adhesive was applied through the filler holes, as shown in Figure 4b. This method of forcing the adhesive into the bottom of the hole and allowing it to flow to the top opening avoids formation and entrapment of air bubbles along the bonded length. The adhesive used in this study to fill the holes was the CI-LV FS epoxy (Simpson Strong-Tie 2023b).

Once the GiRs were installed in Part B and allowed to cure, the element was lifted and placed on top of Part A, such that the assembled specimen rested upside down (Figure 4a and Figure 4c) relative to how it is shown in Figure 3. The adhesive was then injected through the filler hole and flowed out the weep hole in Part A, as indicated in Figure 4c. As expected, some weep holes were not sufficient to drain all the adhesive being injected, and in some cases, adhesive would overflow and cure at the joint interface (Figure 4b). The effect of the excess adhesive in the joint interface is further discussed in the results section. While the two-stage adhesive application involved applying CI-LV FS epoxy over cured CI-GV gel epoxy, limited published data exists on the bond characteristics between these specific epoxy systems. The manufacturer's technical documentation does not indicate incompatibility between these products, and both are epoxy-based adhesives designed for structural applications. Post-test observations confirmed adequate bonding at the rod-to-timber interface in all specimens, with no evidence of delamination between adhesive layers.

Once fabricated, specimens were stored inside OSU's Structural Engineering Research Laboratory at ambient temperature for 2 months prior to testing. The moisture content of the specimens was measured at the time of testing and had a mean value of 11.7% and a coefficient of variation of 4.7%, measured using a handheld surface moisture meter.

Test setup

Figure 5 shows an elevation and section view of the self-reacting test setup design. The main components include base connections, actuator and load cell, a transition W-shape section, a steel reaction buttress, the primary support beam, and out-of-plane restraints. Part B of each MPP specimen was restrained using steel connections to a 6096 mm (20 ft) long W14x159 reaction beam indicated as primary support beam.

The MPP specimen was attached to an actuator positioned so that the centerline of the actuator force was at the same elevation as the specimen joint interface. A 32 mm × 127 mm × 673 mm (1-1/4 in. × 5 in. × 26-1/2 in.) steel plate was inserted

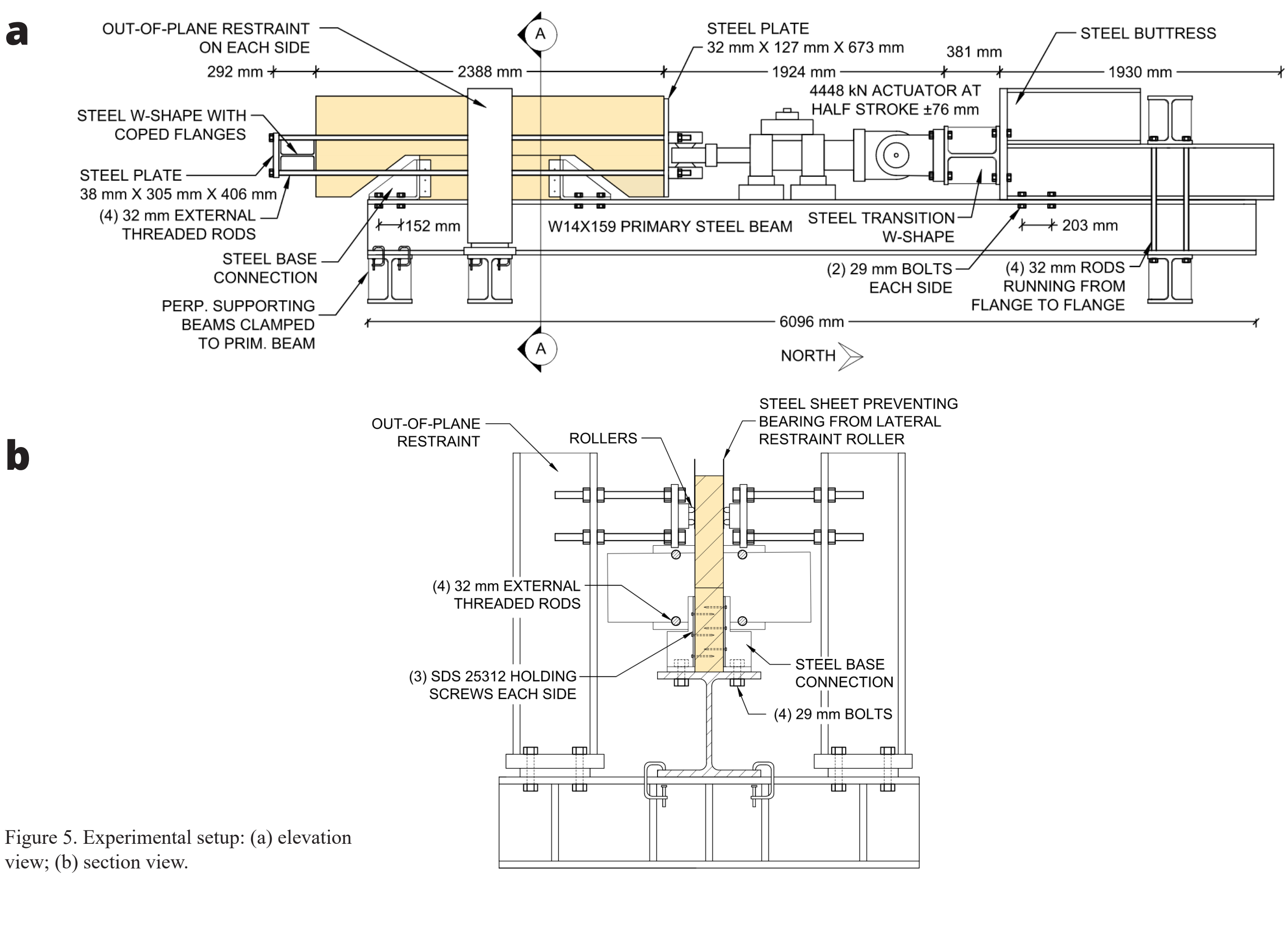

Figure 5. Experimental setup: (a) elevation view; (b) section view.

between the face of the actuator and the end of the MPP specimen to uniformly distribute the applied load and prevent fiber crushing at the load application point. Four 32 mm (1-1/4 in.) diameter steel rods connected the actuator at the north end of the specimen to a wide-flange beam at the south end of the specimen to allow the specimens to be pushed and pulled by the actuator. The actuator was attached to a steel reaction buttress. The buttress was restrained to the primary support beam with four 28.6 mm (1-1/8 in.) diameter steel bolts and additional wrench clamps. The bolts were spaced at 203 mm (8 in.) on-center and placed at the south end of the buttress. To promote lateral stability of the reaction, a W12x120 section was placed on top of the north end of the buttress and tensioned to another W12x120 section that was oriented perpendicular to the supporting beam beneath. The MPP specimen and steel buttress rested upon and were restrained to the primary support beam. The MPP specimen was attached to the primary support beam by means of a steel base connection that was bolted to the beam and screwed to the MPP specimen, using SDS 25312 holding screws. Underneath the primary support beam were three perpendicular W12x120 beams that were clamped to the primary support beam to provide lateral stability for the primary support beam.

To facilitate in-plane movement of the MPP specimen during testing, out-of-plane restraints were added to both sides of the specimen, as shown in Figure 5b. This restraint mechanism included roller bearings that allowed for Part A of the MPP specimen to move in-plane with minimal resistance, while restricting out-of-plane motions. In addition, two 1.5 mm thick steel bearing plates were fastened to either side at the contact point of the roller to prevent direct roller contact with the MPP.

Instrumentation setup

The responses of MPP specimens during interface shear tests were monitored with six instruments. Four sensors were used to measure the relative displacements between the top and bottom elements across the joint of the specimen, as shown in Figure 6, and two other sensors tracked the actuator-applied load and actuator displacement. Two displacement sensors (string potentiometers), SP1 and SP2, on the east and west face, respectively, measured horizontal relative displacements between Part A and B, and two linear potentiometers (Duncan-type potentiometers), labeled SP3 and SP4, measured relative vertical displacements between Part A and Part B.

Testing protocols

Testing featured two loading protocols. The first was a displacement-controlled monotonic loading protocol, and the second was a force-controlled reversed cyclic loading protocol. Figure 7a shows the monotonic loading protocol applied in accordance with ISO 6891 (ISO 1983). Under this first monotonic loading protocol, two specimens were tested. A F_{est} value of 89 kN was used for the two monotonic tests. The initial actuator displacement rate was first set at 2.5 mm/min, increased to 7.6 mm/min after 12.7 mm was reached, and lastly increased to 12.7 mm/min after 31.8 mm displacement was achieved. The last displacement rate of 12.7 mm/min was maintained until the post-peak load had reduced to 80% of peak load or until the maximum stroke of the actuator was reached (~ ±75 mm), whichever occurred first.

Reversed-cyclic loading was performed in accordance with a force-controlled CUREE protocol (Krawinkler et al. 2001), as shown in Figure 7b, where the Q_0 value was set to the average peak load obtained from monotonic testing. Cyclic testing included nine specimens. The first cyclic test began at a displacement rate of 5.1 mm/min, was increased to 10.2 mm/min after five cycles, then was increased to 20.3 mm/min after another five cycles and maintained at this latter level for the remainder of the test. Subsequent cyclic tests for specimens numbered 2 to 9 were performed at a displacement rate of 20.3 mm/min for the entirety of the test.

Data post-processing and reduction

Two monotonic tests were conducted to determine a reference force value Q_0 to be used for the reversed-cyclic loading. Reported results from the monotonic tests include peak load, displacement at peak load, and the yield strength (to be discussed more in the next section). The reported values for the cyclic tests include the peak load (kN), number of cycles to reach the peak load (#), and the cyclic elastic stiffness (kN/mm). The first two parameters are self-explanatory. However, for the cyclic elastic stiffness, multiple definitions could be used. The elastic stiffness was determined by taking the average of the slope of the pushing phase for cycles 2 to 4 of the load versus displacement graph, corresponding to regions highlighted in Figure 7b.

Reporting guidelines for experimental tests involving GiRs in wood structural elements are also provided in ICC-AC526 (ICC-ES 2021). While this document primarily relates to strength in tension for this connection type, the allowable loads in shear were determined using the definitions in the acceptance criteria document, including: *nominal shear strength*, which is the average of the peak loads; *allowable GiR shear capacity*, which is the nominal shear strength divided by a safety fac-

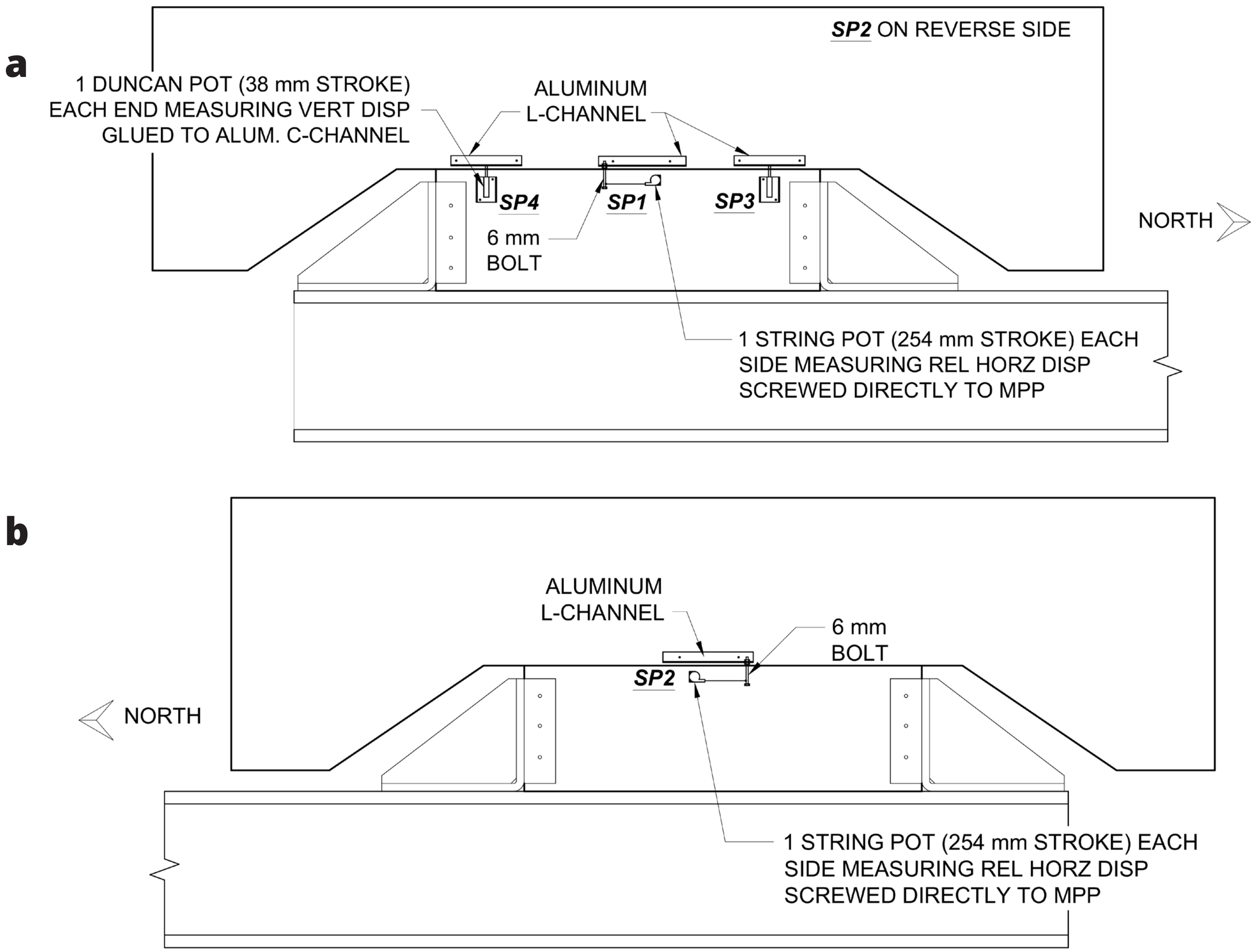

Figure 6. Instrumentation setup: (a) east face of the specimen; (b) west face of the specimen.

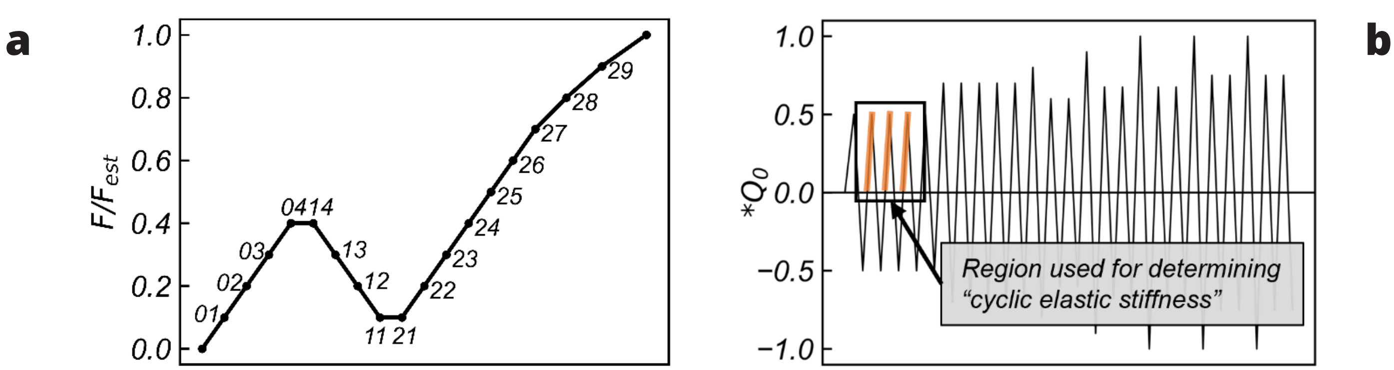

Figure 7. Loading protocols used in testing: (a) monotonic loading per ISO 6891; (b) force-controlled CUREE cyclic testing and selected quarter-cycles used to determine the cyclic elastic stiffness.

tor equal to 5; and *available GiR strength in LRFD*, which is determined by using a format conversion factor, K_F, of 3.32, a resistance factor, φ, of 0.65, and a time effect factor, λ, of 1.00, all applied to the allowable GiR shear capacity. The format conversion factor, resistance factor, and time effect factor were determined in accordance with Table N3.3 in Appendix N of the 2018 NDS (AWC 2018).

Yield strength determination

The ability of the NDS equations to predict the yield strength of this connection type was examined through comparison with the yield strengths obtained from the monotonic tests. While several approaches for determining yield strength are available for timber connections (Kržan et al. 2023), two commonly used methods in North America were selected for this study: (1) the 5% offset method described in ASTM D5764 (ASTM International 2018); and (2) the equivalent energy elastic-plastic (EEEP) method described in ASTM E2126 (ASTM International 2005). The 5% offset method defines the yield point as the intersection of the load-deformation response with a line offset from the initial elastic stiffness by 5% of the fastener diameter, and it is commonly used for dowel-type connection testing and comparison with NDS yield predictions. In contrast, the EEEP method determines the yield point by using a bilinear idealization of the load-deformation response with equivalent energy dissipation, and it is widely used in cyclic connection testing and structural performance assessment. Both methods were used in this study to facilitate comparison with prior GiR connection research and to evaluate the sensitivity of the calculated yield strength to the selected interpretation method. Each specimen contained three rods; therefore, the predicted yield strength reported for the connection was taken as three times the predicted yield strength of a single rod.

The GiR connections in this study were loaded in interface shear, with each rod crossing the MPP panel-to-panel splice and loaded transversely to its longitudinal (strong) axis. This loading configuration is mechanically analogous to a single-shear dowel connection between two wood members, for which the EYM, as implemented in the NDS (AWC 2018), is directly applicable. The term "longitudinal splice" refers to the geometric arrangement of the panels, which were joined along their length and major strength axis, rather than to the loading direction relative to the rod. Because the load transfer mode (transverse rod loading) was consistent with EYM assumptions, the NDS yield limit equations were used to predict the reference lateral design values for the GiR connection.

Experimental results and discussion

Test results for the two specimens subjected to monotonic loading and nine specimens subjected to cyclic loading are reported in this section. In addition, comparison of the test results to existing design equations and use of acceptance criteria are described to facilitate future designs using these test results.

Monotonic loading test results

The first phase of testing featured two monotonic tests (MT1-2) to determine the specimen yield strength and reference force value (Q_0) for the cyclic CUREE protocol. The respective peak load and displacement at peak load recorded were 122 kN and 24.9 mm, and 126 kN and 16.5 mm, for an average peak load of 124 kN. Figure 8 shows the applied load versus interface relative horizontal displacement for both tests, where the displacement values were reported as the average of the SP1 and SP2 sensor displacements.

The yield strength for monotonic tests was calculated and compared using the 5% offset method and EEEP method. For the 5% offset method, the calculated yield strengths for the tests were 110 kN and 85 kN, for an average of 97.5 kN. For the EEEP method, yield strength values of 102 kN and 113 kN were calculated, for an average of 107.5 kN. Monotonic test results are summarized in Table 2.

Cyclic loading test results

The second phase of testing featured nine fully reversed-cyclic tests (CT1-9), where testing started on the pushing stroke, i.e., with the actuator applying a force on the specimen in the south

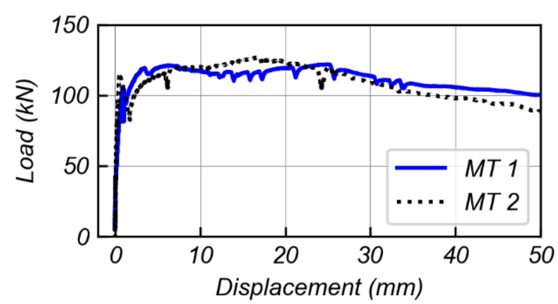

Figure 8. Monotonic tests: load versus relative horizontal displacement of the joint.

Table 2. Summary of monotonic test results.

MT No.	Peak load (kN)	Displacement at peak load (mm)	Yield strength, 5% offset (kN)	Yield strength, EEEP (kN)
1	122	24.9	110	102
2	126	16.5	85	113
Mean	124	20.7	97.5	107.5

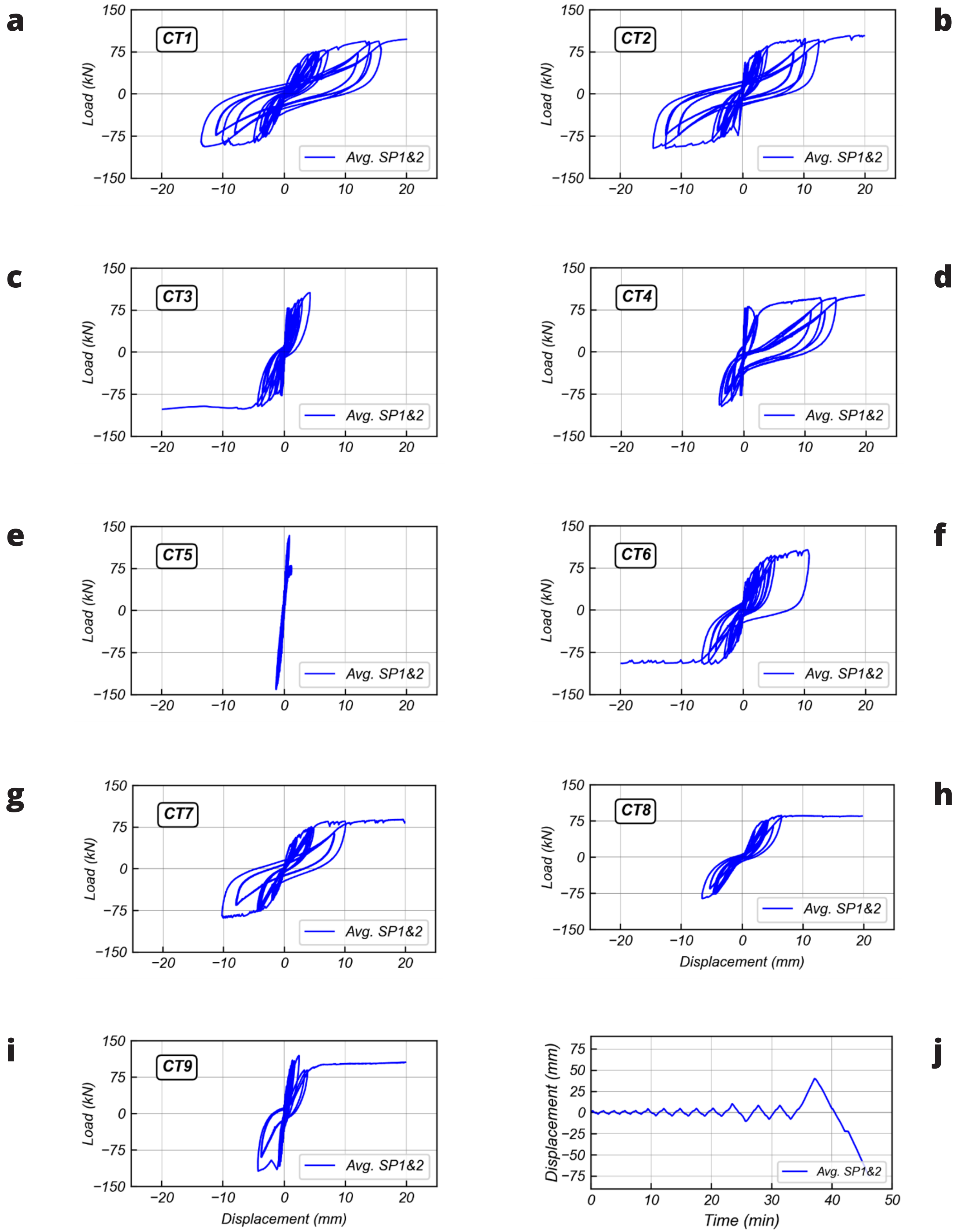

Figure 9. Measured load versus relative horizontal displacement along splice for all specimens tested under cyclic loading and example displacement versus time plot for specimen CT7.

direction. Figure 9a to Figure 9i show hysteresis plots, with recorded actuator loads versus the average of SP1 and SP2 relative horizontal displacement measurements at the joint interface, for the nine specimens plotted until 20 mm of relative displacement. It can be observed from these responses that CT3 and CT6 reached 20 mm on the pulling (negative) direction, while CT1, 2, 4, 7, 8, and 9 reached 20 mm on the pushing stroke. However, for CT5, the adhesive bond was not seen to fail prior to Part A twisting out-of-plane, leading to an early termination of testing, and no appreciable inelastic response. Figure 9j presents the relative joint displacement versus time plot for a representative specimen, where the largest relative displacements can be observed during the final cycle of testing.

The peak load and elastic stiffness values obtained from the cyclic tests exhibited two distinct groupings, hereafter referred to as "Cluster 1" and "Cluster 2". Figure 10 illustrates the separation of data into the two clusters, while the corresponding response values are summarized in Table 3 and Table 4, respectively.

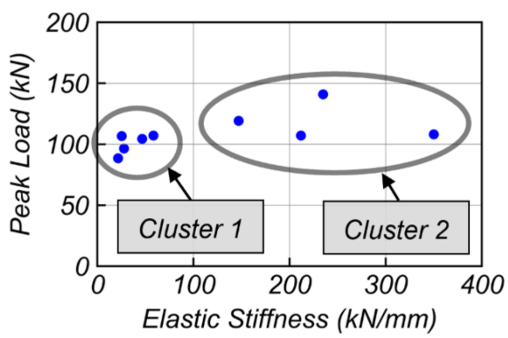

Figure 10. Clustering of cyclic test results.

Table 3. Cluster 1 test results.

CT no.	Peak load (kN)	Number of cycles to peak load	Elastic stiffness (kN/mm)
1	106.8	20.5	25.4
2	104.5	20	46.7
6	107.2	23	58.5
7	96.5	14.5	27.8
8	88.5	14	21.7
Mean	**100.7**	**18.4**	**36.0**
COV	*7.2%*	19.2%	39.3%

Table 4. Cluster 2 test results.

CT no.	Peak load (kN)	Number of cycles to peak load	Elastic stiffness (kN/mm)
3	107.2	23	212
4	108.1	29.5	350
5	141.0	38	235
9	119.2	28	147
Mean	**118.8**	**29.6**	**236**
COV	*11.5%*	*18.2%*	*31.1%*

The unintended accumulation of epoxy at the MPP panel-to-panel interface in a subset of specimens resulted in partial adhesive bonding across the interface, altering the load transfer mechanism from a purely mechanical dowel action to a combined adhesive-mechanical system. Because the goal of this study was to characterize the capacity of the mechanical GiR connection alone, the two groups were analyzed separately, with Cluster 1 providing the basis for the proposed design values. Accordingly, statistical comparisons were used primarily to identify trends, rather than to establish definitive population-level differences. Specimens exhibiting the additional interface epoxy (Cluster 2) consistently achieved higher peak loads than those without it (Cluster 1). Even with four to five specimens per cluster, the COVs of the peak loads were relatively small (7.2% for Cluster 1 and 11.5% for Cluster 2). Statistical comparison using a one-tailed t-test for two independent means indicated significant differences ($p < 0.05$) between the clusters in terms of peak load, elastic stiffness, and number of cycles to peak load (p-values = 0.0290, 0.000588, and 0.00651, respectively).

As mentioned, the differences observed between the two clusters are suspected to be attributable to variations in joint interface conditions resulting from specimen fabrication and assembly. Figure 11 and Figure 12 present representative pre-test and post-test interface conditions for a Cluster 1 specimen (CT8), while Figure 13 and Figure 14 show corresponding views for a Cluster 2 specimen (CT5). A comparison of the pre-test conditions shown in Figure 11 and Figure 13 indicates that Cluster 1 specimens generally exhibited a larger interface gap, within expected construction tolerances. Post-test observations further suggest that Cluster 2 specimens tended to accumulate epoxy between the adjoining parts near the GiRs, allowing an adhesive bond to develop across portions of the interface. This unintended adhesive contribution is therefore suspected to have altered the load transfer mechanism and contributed to the observed differences in response between the two clusters. Although the adhesive bond appeared to increase peak load capacity, its influence on elastic stiffness was substantially more pronounced.

Cluster 1 and 2 were also compared in terms of energy dissipation. Figure 15 illustrates the cumulative energy dissipation per cycle of testing. Energy dissipation per cycle was computed as the area enclosed by each load-deformation

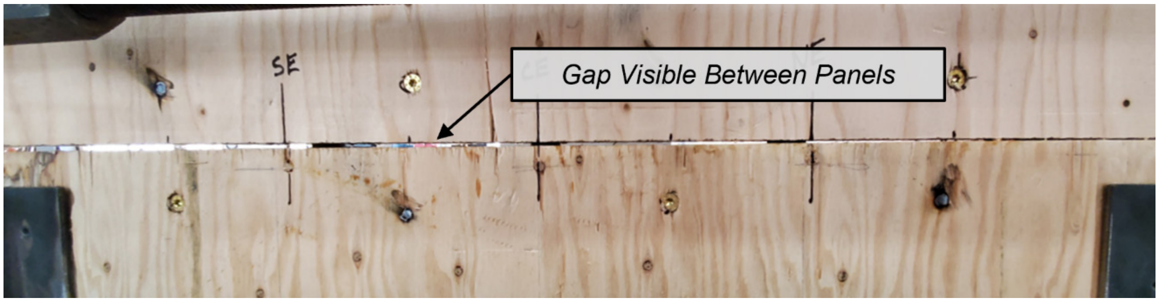

Figure 11. Example joint condition before testing for specimens in Cluster 1, showing visible gap between top and bottom elements (specimen from CT8 shown).

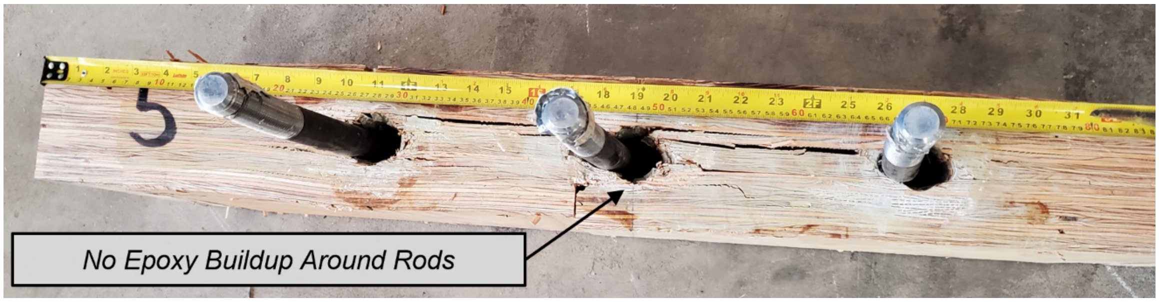

Figure 12. Example of panel interface after testing for specimens in Cluster 1 (specimen from CT8 shown).

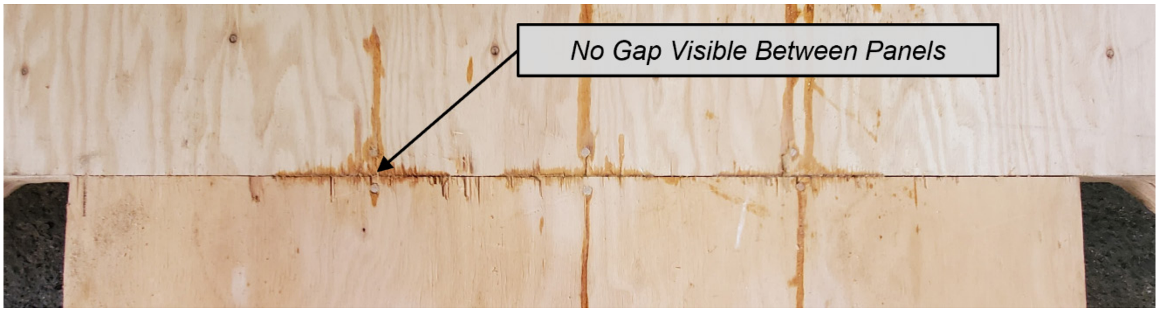

Figure 13. Example joint condition before testing for specimens in Cluster 2 (specimen from CT5 shown).

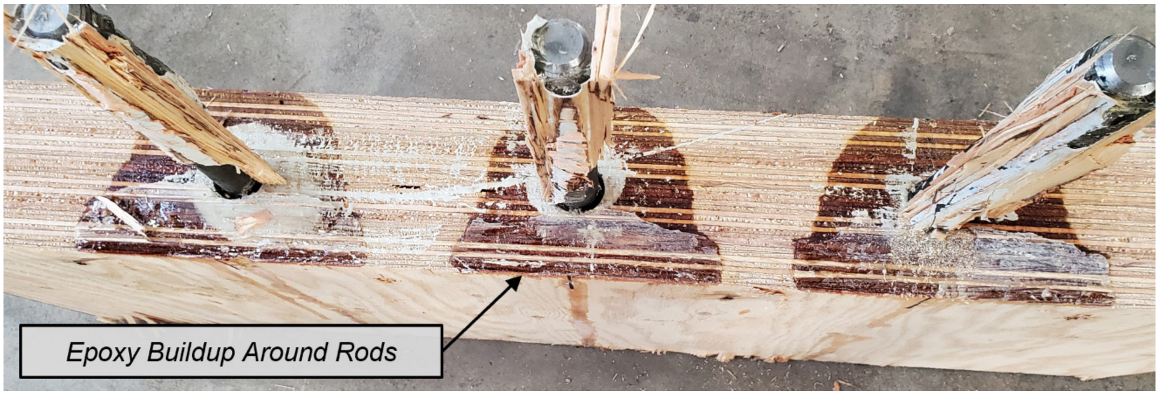

Figure 14. Example of panel interface after testing for specimens in Cluster 2 (specimen from CT5 shown).

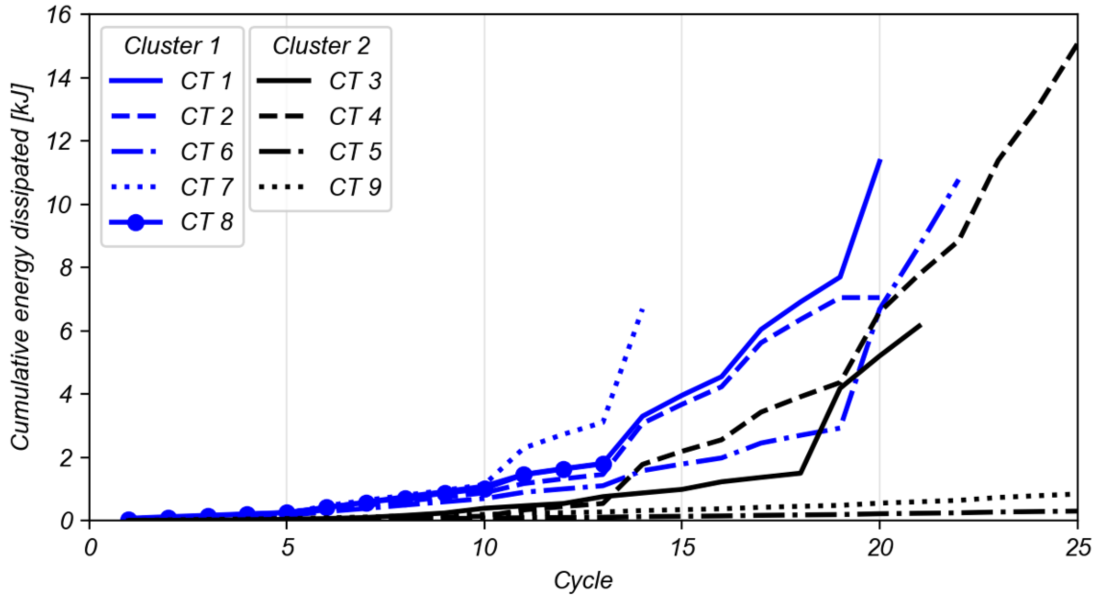

Figure 15. Cumulative energy dissipated in each cyclic test sorted by cluster.

hysteresis loop using trapezoidal integration of the recorded data, and the cumulative energy dissipation, i.e., the running sum of the per-cycle loop areas, was reported for the first 25 cycles of each test under the CUREE protocol. The purpose of this comparison was to evaluate the onset and accumulation of energy dissipation for the two interface conditions. Cluster 1 specimens dissipated energy from the early cycles of loading, whereas Cluster 2 specimens exhibited a delayed onset of energy dissipation, consistent with their initially stiffer, adhesive-dominated response prior to yielding (with CT5 and CT9 dissipating little energy). Given the limited number of specimens per cluster, statistical comparisons were used primarily to identify trends as discussed previously.

The condition of the GiRs was examined by dissecting the specimens at the conclusion of the tests. Some specimens contained rods that exhibited bending with a single plastic hinge located in Part A (yield mode III), while two plastic hinges were observed to have formed in other specimens (yield mode IV). Figure 16a shows an example specimen cross-section from CT3 displaying the formation of a single plastic hinge. Figure 16b shows an example specimen from CT2, where two plastic hinges can be observed. Plastic hinge formation was observed to occur at approximately 75 mm up/down from the joint interface. No significant correlation was found between yield mode and structural response of the connection.

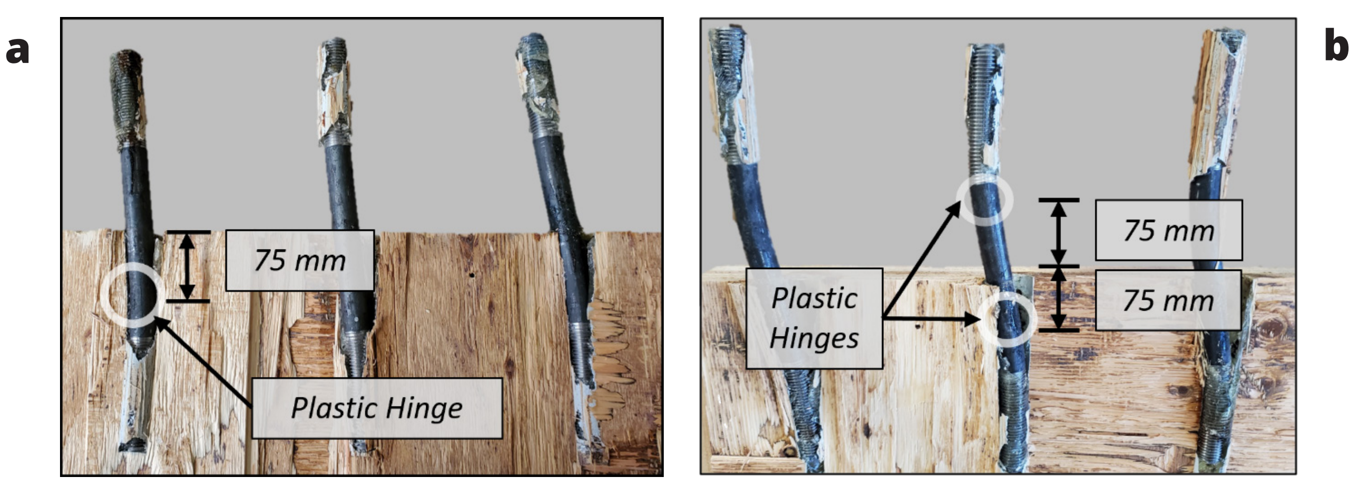

Figure 16. Cross section of dissected specimens: (a) CT3 exhibiting yield mode III; and (b) CT2 exhibiting yield mode IV.

Discussion and design values

The two clusters observed in the data demonstrate that the interface condition had a substantial influence on connection response. Specimens observed to contain epoxy accumulation at the panel interface (Cluster 2) were associated with increased peak load and elastic stiffness, relative to specimens without observed epoxy accumulation (Cluster 1). It is suspected that this behavior can be attributed to a combined adhesive-mechanical load transfer mechanism in Cluster 2, whereas Cluster 1 specimens were governed primarily by mechanical dowel action.

The distinction between the two clusters is important from a design perspective. Although the additional interface adhesion increased connection capacity, the amount of adhesive engagement was dependent on fabrication tolerances and epoxy accumulation that could not be reliably controlled or quantified using the proposed installation procedure. Consequently, reliance on this unintended adhesive contribution could lead to unconservative design assumptions. Because the objective of this study was to characterize the performance of the GiR connection itself, Cluster 1 specimens were considered more representative of the intended mechanical connection behavior and therefore provide a more appropriate lower-bound basis for the proposed design values.

Utilizing results from the Cluster 1 specimens, design values were calculated following the procedures established in ICC-AC526 (ICC-ES 2021) and described in the Data post-processing and reduction section. The nominal shear strength, taken as the mean peak load, was calculated as 100.7 kN for the 3-GiR connection and 33.6 kN for a single GiR. Applying the prescribed safety factor of 5 resulted in allowable GiR shear capacities of 20.1 kN and 6.7 kN for the 3-GiR connection and a single GiR, respectively. The available shear strengths in LRFD were determined by applying format conversion factors to the allowable values, resulting in available strengths of 43.5 kN for the 3-GiR connection and 14.5 kN for a single GiR.

The reference lateral design values from the NDS were calculated to compare with experimentally derived design values (AWC 2018). For this calculation, the predicted yield strength was first determined using NDS yield equations presented in Table 1, and a dowel bearing strength of 18 MPa for MPP loaded in-plane, with veneers oriented perpendicular to the major strength direction (Miyamoto et al. 2020). NDS yield mode IV governed this calculation and produced a predicted yield strength of 85.3 kN for the 3-GiR connection. Finally, a reduction value ($R_d = 4$) was applied per Equation [1], and a reference lateral design value of 21.3 kN was obtained (P/R_d), corresponding to 7.1 kN per GiR. This value exceeds the allowable GiR shear capacity by a modest 5.6%. However, it is important to note the difference in the values of the NDS (AWC 2018) reduction term (4.0) and the factor of safety adopted in the ICC-AC526 (5.0, in ICC-ES 2021), which highlights the importance of testing to validate predicted and design values. Table 5 summarizes results for the nominal shear strength, allowable GiR shear capacity, available GiR strength in LRFD, and the NDS calculated reference lateral design value for the 3-GiR connection and for a single GiR.

The NDS predicted yield strength (AWC 2018) was also compared to experimentally derived yield strength values (presented in Table 2). This comparison showed that the mean values of the 5% offset and EEEP methods exceeded the NDS prediction by 14% and 26%, respectively. From pre-test visual inspection, it was suspected that monotonic specimens may also be influenced by adhesion at the interface. To confirm, a one-tailed t-test for two independent means was performed to

Table 5. Derived and predicted design values for Cluster 1 specimens.

GiR quantity	ICC-AC526, nominal shear strength (kN)	ICC-AC526, allowable GiR shear capacity (kN)	NDS, reference lateral design value (kN)	ICC-AC526, available GiR strength in LRFD (kN)
3	100.7	20.1	21.3	43.5
1	33.6	6.7	7.1	14.5

Table 6. Comparison of peak load between monotonic and cyclic tests.

Comparison group	Mean peak load (kN)	Difference (%)	p-value	Statistical difference
Monotonic	124	--	--	--
Cyclic (Cluster 1)	100.7	-18.7	0.0063	Significant
Cyclic (Cluster 2)	118.8	-4.2	0.344	Not significant

compare the monotonic test group with the cyclic test groups. It was calculated that the difference between peak load values for monotonic testing and Cluster 1 specimens was statistically significant $p < 0.05$ ($p = 0.0063$), while not statistically significant for Cluster 2 ($p = 0.344$), as summarized in Table 6. This finding agreed with observed joint conditions and provided additional evidence that monotonic testing specimens were similar to Cluster 2 specimens, explaining the higher experimentally derived yield strength. Using a dowel bearing strength of 18 MPa for MPP loaded in-plane with veneers oriented perpendicular to the major strength direction, NDS yield Mode IV (AWC 2018) governs and gives a predicted yield strength of 28.4 kN per rod. The mean experimentally evaluated yield strengths from the monotonic tests were 97.5 kN by the 5% offset method and 107.5 kN by the EEEP method, exceeding the NDS prediction by 14% and 26%, respectively. The comparison is based on the monotonic test results only. Cyclic tests were not included because the CUREE cyclic protocol is intended to characterize ductility and energy dissipation, rather than yield strength, and extracting yield points from a cyclic envelope introduces additional uncertainty. These results indicate that the NDS EYM provides a conservative estimate of the yield strength of the GiR splice connection for the configuration tested.

Several limitations should be acknowledged when interpreting the findings of this experimental program. First, the sample size was limited, and the comparisons presented herein are exploratory in nature and should be interpreted accordingly. Even with four to five specimens per cluster, the coefficients of variation of the peak loads were relatively small (7.2% for Cluster 1 and 11.5% for Cluster 2). Second, the test program addressed a single rod diameter, embedment depth, and adhesive type, so the applicability of the proposed design values to other configurations has not been experimentally verified. Third, all tests were conducted under short-term loading at ambient conditions; the long-term performance of these connections under sustained loads and environmental exposure, such as moisture cycling and temperature variation, remains to be characterized and is identified as a priority for future research. Additionally, the NDS yield capacity predictions presented here use conventional NDS dowel bearing strength values (F_{em}) for MPP (AWC 2018), which do not account for the full dowel-adhesive-wood load transfer sequence characteristic of GiR connections. Prior studies on axially loaded GiR connections have demonstrated that using adhesive-wood interface bearing strength, characterized through dedicated bearing tests, improves the accuracy of EYM predictions. Future work should include bearing tests at the adhesive-MPP interface to refine the EYM-based design methodology for GiR shear connections in veneer-based panel products.

Conclusion

Interface shear tests were performed to characterize the structural behavior of GiRs in MPP. Monotonic loading tests were conducted per ISO 6891 (ISO 1983), and fully reversed-cyclic loading was performed according to a force-controlled CUREE protocol (Krawinkler et al. 2001). The following summarizes the primary findings and key observations from the experimental investigation and subsequent analytical evaluation:

1. Cyclic test results were grouped into two clusters based on a statistically significant difference in measured peak load and elastic stiffness. The mean peak load and elastic stiffness for specimens in Cluster 1 were 100.7 kN and 36.0 kN/mm, respectively, and 118.8 kN and 236 kN/mm for specimens in Cluster 2. From pre- and post-test observations, it is strongly suspected that the condition at the interface of the two parts of the specimens (accumulated adhesive) was the primary factor separating clusters.

2. Cluster 1 was used as the basis for conservative design values because it more closely represented the intended mechanical dowel-action behavior. For a single GiR, the nominal shear strength, allowable GiR shear capacity, and available shear strength in LRFD were calculated as 33.6 kN, 6.7 kN and 14.5 kN, respectively. However, the response observed in Cluster 2 is also informative and may represent an upper-bound condition associated with unintended interface adhesion. Additional testing is needed to more accurately characterize the structural response of this condition.

3. Comparison of experimentally derived design values with NDS-based predictions showed reasonable agreement. Using NDS yield mode IV (AWC 2018) and a dowel bearing strength of 18 MPa for MPP, the predicted reference lateral design value was calculated as 7.1 kN per GiR, which exceeded the experimentally derived allowable GiR shear capacity by 5.6%.

4. The experimentally evaluated yield capacity exceeded the NDS prediction by 14% based on the 5% offset method and by 26% based on the EEEP method (ASTM International 2005), indicating that the NDS EYM provides a conservative estimate of the shear capacity of the GiR splice connection for the configurations tested.

5. The divergence in connection response between Cluster 1 and Cluster 2 specimens underscores the importance of adhesive control during fabrication. Cluster 2 specimens, which had epoxy accumulated at the panel interface, exhibited substantially higher elastic stiffness (mean 236 kN/mm vs. 36.0 kN/mm) and modestly higher peak loads (mean 118.8 kN vs. 100.7 kN) relative to Cluster 1. The interface condition therefore governed stiffness far more than peak load. In both cases, the specimens exhibited ductile behavior consistent with yield modes III and IV. However, the delayed onset of energy dissipation in Cluster 2 reflects the initially stiffer, adhesive-dominated response before yielding. Future testing should explicitly characterize both interface conditions as controlled variables, using separate specimen groups fabricated with and without intentional interface adhesion, to establish distinct design recommendations. In the interim, fabrication protocols should incorporate measures to prevent unintended epoxy accumulation at the panel joint, such as temporary interface spacers or interface sealing prior to rod installation.

6. The findings of this study highlight the sensitivity of GiR shear connection response to interface conditions and fabrication tolerances. Future work should further investigate MPP interface behavior associated with unintended adhesive bonding and develop improved EYM-based prediction methods that better represent the dowel-adhesive-wood load transfer mechanism in veneer-based mass timber products.

Data availability statement

The data and codes generated related to this paper are available from the corresponding author upon reasonable request.

References

Abed J, Rayburg S, Rodwell J, Neave M (2022) A review of the performance and benefits of mass timber as an alternative to concrete and steel for improving the sustainability of structures. Sustainability 14(9):5570. https://doi.org/10.3390/su14095570

APA (2025) ANSI/APA PRG 320-2025 Standard for Performance-Rated Cross-Laminated Timber. https://www.apawood.org/publication-search?q=PRG+320&tid=1

ASTM International (2005) ASTM E2126-05: Standard Test Method for Cyclic (Reversed) Load Test for Shear Resistance of Walls for Buildings. https://store.astm.org/e2126-05.html

ASTM International (2018) ASTM D5764-97a: Standard Test Method for Evaluating Dowel-Bearing Strength of Wood and Wood-Based Products. https://store.astm.org/d5764-97ar18.html

AWC (2014) Technical Report 12: General Dowel Equations for Calculating Lateral Connection Values. https://awc.org/wp-content/uploads/2021/12/AWC-TR12-1510.pdf

AWC (2018) NDS: National Design Specification for Wood Construction. American Wood Council. https://awc.org/wp-content/uploads/2021/10/AWC_NDS2018-withCommentary_20210917_AWCWebsite_TOC.pdf

Ayansola GS, Tannert T, Vallee T (2022). Experimental investigations of glued-in rod connections in CLT. Constr Build Mater 324:126680. https://doi.org/10.1016/j.conbuildmat.2022.126680

Azinović B, Serrano E, Kramar M, Pazlar T (2018) Experimental investigation of the axial strength of glued-in rods in cross laminated timber. Mater Struct 51(6):143. https://doi.org/10.1617/s11527-018-1268-y

Bader TK, Schweigler M, Serrano E, Dorn M, Enquist B, Hochreiner G (2016) Integrative experimental characterization and engineering modeling of single-dowel connections in LVL. Constr Build Mater 107:235–246. https://doi.org/10.1016/j.conbuildmat.2016.01.009

Bengtsson C, Johansson C-J (2002) GIROD - Glued-in Rods for Timber Structures (Nos. SMT4-CT97-2199). Swedish National Testing and Research Institute. https://urn.kb.se/resolve?urn=urn:nbn:se:ri:diva-4586

Deng JX (1997) Strength of Epoxy Bonded Steel Connections in Glue Laminated Timber. PhD thesis, University of Canterbury, Christchurch, NZ. https://dx.doi.org/10.26021/2511

Di Cesare A, Ponzo FC, Lamarucciola N, Nigro D (2020) Experimental seismic response of a resilient 3-storey post-tensioned timber framed building with dissipative braces. Bull Earthq Eng 18:6825–6848. https://doi.org/10.1007/s10518-020-00969-y

Field T, Barbosa AR, Zimmerman, RB, Pryor S, Sinha A, Higgins C (2023) Experimental and analytical evaluation of the tension capacity of edgewise connected glued-in rods in mass ply panels. Constr Build Mater 409:133853. https://doi.org/10.1016/j.conbuildmat.2023.133853

Granello G, Palermo A, Pampanin S, Pei S, van de Lindt J (2020) Pres-Lam buildings: State-of-the-art. J Struct Eng 146(6):04020085. https://doi.org/10.1061/(ASCE)ST.1943-541X.0002603

ICC-ES (2021) Acceptance Criteria for Factory Installed Glued-In Rods in Wood Structural Elements (AC 526). International Code Council (ICC) Evaluation Service. https://icc-es.org/acceptance-criteria/AC526/

ICC-ES (2022) ESR-4760: Freres Mass Ply Panel (MPP). International Code Council (ICC) Evaluation Service. https://icc-es.org/report-listing/esr-4760/

ISO (1983) ISO 6891: Timber Structures—Joints Made with Mechanical Fasteners—General Principles for the Determination of Strength and Deformation Characteristics. https://www.iso.org/standard/13413.html

Izzi M, Casagrande D, Bezzi S, Pasca D, Follesa M, Tomasi R (2018) Seismic behaviour of cross-laminated timber structures: A state-of-the-art review. Eng Struct 170(1):42–52. https://doi.org/10.1016/j.engstruct.2018.05.060

Jensen JL, Gustafsson P-J (2004) Shear strength of beam splice joints with glued-in rods. J Wood Sci 50(2):123–129. https://doi.org/10.1007/s10086-003-0538-6

Jensen JL, Quenneville P (2009) Connections with glued-in rods subjected to combined bending and shear actions. Working Commission CIB-W18–Timber Structures, New Zealand. https://www.researchgate.net/publication/279058056

Johansen KW (1949) Theory of Timber Connections. International Association of Bridge and Structural Engineering 9:249–262 https://doi.org/10.5169/seals-9703

Kontra S, Barbosa AR, Sinha A, Pryor S, Zimmerman RB, Simpson B, van de Lindt JW, Pei S, Araújo R GA. McBain M, Pieroni L, Mishra P, Uarac P PA, Field T, Freddi F (2026) Mass timber wall splice connection using glued-in rods: Design methodology, implementation, and shake-table testing in a six-story building. Eng Struct 361:122859. https://doi.org/10.1016/j.engstruct.2026.122859

Krawinkler H, Parisi F, Ibarra L, Ayoub A, Medina R (2001) Development of a Testing Protocol for Woodframe Structures. CUREE-Caltech Woodframe Project Report W-02, Consortium of Universities for Research in Earthquake Engineering, Stanford Digital Repository. https://purl.stanford.edu/bf933wk8343

Kržan M, Aquino C, Schweigler M, Li Z, Branco J (2023) Protocols and results analysis methods for cyclic tests of timber joints. A discussion. In: Proc. World Conference on Timber Engineering (WCTE), 19–23 June 2023, Oslo, Norway, pp. 3685–3693. https://doi.org/10.52202/069179-0479

Miyamoto BT, Sinha A, Morrell I (2020) Connection performance of mass plywood panels. For Prod J 70(1):88–99. https://doi.org/10.13073/FPJ-D-19-00056

NZS 3603 (1993) Timber Structure Standard. In: Standards Association of New Zealand. https://codehub.building.govt.nz/resources/36031993nzs

Pei S, Ryan K, Berman J, Van De Lindt JW, Pryor S, Huang D, Wichman S, Busch A, Roser W, Wyn SL, Ji Y, Hutchinson T, Sorosh S, Zimmerman RB, Dolan J (2024) Shake-table testing of a full-scale 10-story resilient mass timber building. J Struct Eng 150(12):04024183. https://doi.org/10.1061/JSENDH.STENG-13752.

Pei S, Van De Lindt JW, Popovski M, Berman JW, Dolan JD, Ricles J, Sause R, Blomgren H, Rammer DR (2016) Cross-laminated timber for seismic regions: Progress and challenges for research and implementation. J Struct Eng 142(4):E2514001. https://doi.org/10.1061/(ASCE)ST.1943-541X.0001192

Simpson Strong-Tie (2023a) CI-GV Gel-Viscosity Injection Epoxy: Technical Guide. https://www.strongtie.com/epoxyinjection_crackrepairrps/cigv_epoxy/p/ci-gv

Simpson Strong-Tie (2023b) CI-LV Low-Viscosity Injection Epoxy: Technical Guide. https://www.strongtie.com/restorationsolutions_anchoringsystems/cilv_epoxy/p/ci-lv

Sofi M, Lumantarna E, Hoult R, Mooney M, Mason N, Lu J (2021) Bond strength of GiR in cross-laminated timber: A preliminary study. Constr Build Mater 301, 123864. https://doi.org/10.1016/j.conbuildmat.2021.123864

Stamatopoulos H, Massaro FM, Qazi J (2022) Mechanical properties of laterally loaded threaded rods embedded in softwood. Eur J Wood Wood Prod 80(1):169–182. https://doi.org/10.1007/s00107-021-01747-6

Steiger R, Gehri E, Widmann R (2007) Pull-out strength of axially loaded steel rods bonded in glulam parallel to the grain. Mater Struct 40(1):69–78. https://doi.org/10.1617/s11527-006-9111-2

Steiger R, Serrano E, Stepinac M, Rajčić V, O'Neill C, McPolin D, Widmann R (2015) Strengthening of timber structures with glued-in rods. Constr Build Mater 97:90–105. https://doi.org/10.1016/j.conbuildmat.2015.03.097

Sun X, He M, Li Z, Lam F (2020) Seismic performance of energy-dissipating post-tensioned CLT shear wall structures I: Shear wall modeling and design procedure. Soil Dyn Earthq Eng 131:106022. https://doi.org/10.1016/j.soildyn.2019.106022

Tannert T, Follesa M, Fragiacomo M, Gonzalez P, Isoda H, Moroder D, Xiong H, van de Lindt J (2018) Seismic design of cross-laminated timber buildings. Wood Fiber Sci 50:3–26. https://wfs.swst.org/index.php/wfs/article/view/2720

Tlustochowicz G, Serrano E, Steiger R (2011) State-of-the-art review on timber connections with glued-in steel rods. Mater Struct 44(5):997–1020. https://doi.org/10.1617/s11527-010-9682-9

Townsend PK, Buchanan AH, Moss PJ (1990) Steel dowels epoxy bonded in glue laminated timber. Research report, Department of Civil Engineering, University of Canterbury, Christchurch, NZ. https://natlib.govt.nz/records/21926315

Uibel T, Blaß HJ (2006) Load carrying capacity of joints with dowel type fasteners in solid wood panels. International Council for Research and Innovation in Building and Construction: Working Commission W18 - Timber Structures, Paper 39-7-5, Proc. CIB-W18 Meeting 2006, Florence, Italy. https://doi.org/10.5445/IR/1000005149

Xu B-H, Guo J-H, Bouchaïr A (2020) Effects of glue-line thickness and manufacturing defects on the pull-out behavior of glued-in rods. Int J Adhes Adhes 98:102517. https://doi.org/10.1016/j.ijadhadh.2019.102517

Zimmerman RB, Blomgren H-E, McCutcheon J, Sinha A (2020) Catalyst - A mass timber core wall building with high ductility hold-downs in a seismic region. In: Proc. 2020 World Conference on Timber Engineering (WCTE), 24–27 August 2020, Santiago, Chile. https://www.researchgate.net/profile/Hans-Erik-Blomgren/publication/344445838_Catalyst_-_A_Mass_Timber_Core_Wall_Building_with_High_Ductility_Hold-Downs_in_a_Seismic_Region/links/6115baf91e95fe241aca4b71/Catalyst-A-Mass-Timber-Core-Wall-Building-with-High-Ductility-Hold-Downs-in-a-Seismic-Region.pdf